JOURNAL OF Materials CHEMISTRY

Synthesis, structure and properties of a semivalent iron oxoborate, Fe_2OBO_3†

J. P. Attfield,*[a,b] A. M. T. Bell,[a] L. M. Rodriguez-Martinez,[a,b] J. M. Greneche,[c] R. Retoux,[d] M. Leblanc,[d] R. J. Cernik,[e] J. F. Clarke[f] and D. A. Perkins[f]

[a]*Department of Chemistry, University of Cambridge, Lensfield Road, Cambridge, UK CB2 1EW. E-mail: jpa14@cam.ac.uk*
[b]*IRC in Superconductivity, University of Cambridge, Madingley Road, Cambridge, UK CB3 0HE*
[c]*Laboratoire de Physique de l'Etat Condensé, UPRESA CNRS 6087, Université du Maine, 72085 Le Mans, France*
[d]*Laboratoire des Fluorures, UPRESA CNRS 6010, Université du Maine, 72017 Le Mans, France*
[e]*SRS, Daresbury Laboratory, Warrington, UK WA4 4AD*
[f]*Chemical Crystallography Laboratory, University of Oxford, 9 Parks Road, Oxford, UK OX1 3PD*

Received 30th April 1998, Accepted 18th June 1998

Transition metal oxoborates are of interest for magnetic and optical properties. Crystals of many $M^{II}_2M^{III}O_2BO_3$ and $M^{II}M^{III}OBO_3$ materials can be grown from borate fluxes. In the Fe^{II}–Fe^{III}–B–O system, flux growth results in $Fe_3O_2BO_3$ crystals, but solid state reaction at higher temperatures has yielded Fe_2OBO_3 as a polycrystalline powder. This has been characterised by synchrotron and neutron diffraction, electron microscopy, Mössbauer spectroscopy, and conductivity and magnetic measurements. Two notable transitions occur, a broad semiconductor–semiconductor change accompanied by a structural transition at 317 K, and L-type ferrimagnetic order below a Curie temperature of 155 K. An average $(Fe^{2+})_{0.5}(Fe^{3+})_{0.5}$ valence is observed at the two crystallographically distinct sites in Fe_2OBO_3, indicating that charge ordering occurs.

Introduction

Many mixed metal oxoborates $M^{2+}M'^{3+}OBO_3$ adopt the orthorhombic warwickite ($Mg_{1.5}Ti_{0.5}BO_4$) structure,[1,2] including the boron ferrites $MFeOBO_3$ (M = Fe, Co, Ni, Mg) originally reported by Bertaut *et al.*[3] The electronic and magnetic properties of the mixed valent iron compound Fe_2OBO_3 have never been investigated. The similarity of this composition to that of magnetite, Fe_3O_4, which is the parent phase of the spinel ferrites and is of interest for its magnetotransport properties including recently reported magnetoresistance effects,[4] has led us study this phase. In this paper we report the synthesis and structural characterisation of Fe_2OBO_3. A summary of the magnetic and electronic measurements is also given; further details of these properties will appear elsewhere.[5]

Synthesis

A number of attempts were made to prepare crystals of Fe_2OBO_3. Many oxoborates can be crystallised from borate melts, however all attempts to prepare Fe_2OBO_3 in borax fluxes were unsuccessful. Reduction of Fe_2O_3 (1.0 mmol) with Fe powder (1.2 mmol) in 6.0 mmol of anhydrous borax ($Na_2B_4O_7$) flux at 825 °C for 48 h followed by slow cooling to room temperature gave iron oxides as the only crystalline products. Electrolysis of Fe_2O_3 in an excess of anhydrous borax at 850 °C also gave no crystalline oxoborate products. Reduction of 24 mmol Fe_2O_3 and 30 mmol $Na_2B_4O_7$ by 50 mmol hydrogen gas at 900 °C followed by slow cooling under argon gave crystals of a black product. This was found to be the structurally related ludwigite phase $Fe_3O_2BO_3$, for which a single crystal study has previously been reported.[6]

†Basis of the presentation given at Materials Chemistry Discussion No. 1, 24–26 September 1998, ICMCB, University of Bordeaux, France.

Fe_2OBO_3 was successfully prepared as a polycrystalline powder by ceramic methods without sample melting. A phase pure sample was obtained as follows. Fe_2O_3 powder (32.2 mmol) and 64.3 mmol of crystalline H_3BO_3 were ground, pelleted and heated to 700 °C. The nominal '$FeBO_3$' product of this reaction was ground with stoichiometric quantities of Fe powder and Fe_2O_3, and pellets of this mixture were sealed in an evacuated silica glass tube and heated at 1050 °C for 4 days. The black product was found to contain only Fe_2OBO_3 and Fe_3O_4, and no other crystalline borates were observed. The Fe_3O_4 was removed by passing a permanent magnet over the finely powdered sample giving *ca.* 5 g of Fe_2OBO_3 with no secondary phases evident by powder X-ray diffraction. This sample was used in all of the following experiments.

Powder X-ray diffraction

Most warwickite type borates have orthorhombic symmetry (space group *Pmcn*), for example, $Mg_{1.5}Ti_{0.5}OBO_3$,[2] $NiScOBO_3$,[7] $ZnFeOBO_3$,[8] $FeCoOBO_3$,[9] $Co_{1.5}Ti_{0.5}OBO_3$,[10] $Co_{1.5}Zr_{0.5}OBO_3$,[10] $FeMnOBO_3$,[11] $MgAlOBO_3$[12] and $MgScOBO_3$,[13] although monoclinically distorted structures have been reported for $MnAl_{0.5}Y_{0.5}OBO_3$,[8] Mn_2OBO_3,[14] and $Mg_{0.76}Mn_{1.24}OBO_3$.[13] To determine the symmetry for Fe_2OBO_3, a high resolution synchrotron X-ray powder pattern was recorded on instrument X7A at the NSLS, Brookhaven National Laboratory, USA. A scan over $2\theta = 3$–$49.5°$ at a wavelength of 0.7509 Å clearly enables monoclinic splittings to be seen (Fig. 1). The Rietveld-refined cell parameters ($P2_1/c$ symmetry) are $a = 3.17712(7)$ Å, $b = 9.3905(2)$ Å, $c = 9.2455(2)$ Å, $\beta = 90.166(1)°$ at room temperature.

The small β angle suggested that a monoclinic–orthorhombic phase change may take place at high temperatures, and so a further synchrotron powder diffraction experiment was performed. The sample was mounted in a glass capillary and in the GTP furnace on station 9.1[15] of the Daresbury Synchrotron

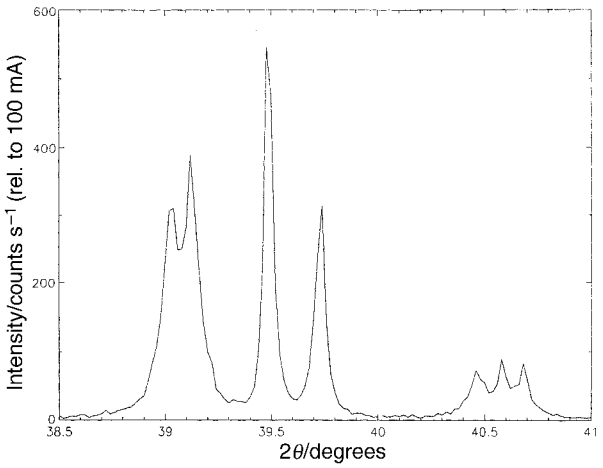

Fig. 1 Part of the high resolution synchrotron X-ray powder diffraction pattern of Fe_2OBO_3 showing the monoclinic splitting of the 102 and $\bar{1}02$ reflections at 39.0 and 39.1° 2θ.

Radiation Source. Scans over the monoclinically split $102/\bar{1}02$ doublet were performed between 285 and 373 K to locate the phase transition. Fig. 2 shows the thermal variation of the full-width at half maximum of this peak, demonstrating that the structure changes to *Pmcn* orthorhombic symmetry at 317 K. Scans over a wider angular range were then recorded at 291, 304, 312, 315, 318 and 337 K for Rietveld fitting, giving the results in Tables 1–3. The cell parameters were refined in each case but poor counting statistics resulted in low precision

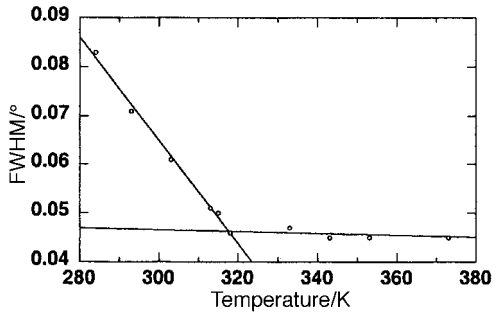

Fig. 2 Thermal variation of FWHM for the combined $102/\bar{1}02$ reflection doublet showing the monoclinic–orthorhombic transition at 317 K.

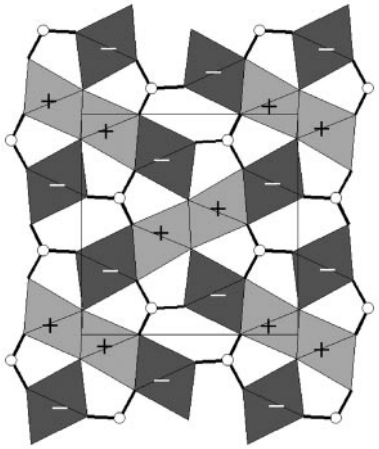

Fig. 3 (100) projection (*b* vertical, *c* horizontal) of the Fe_2OBO_3 structure showing the trigonal planar BO_3 groups and crystallographically independent $Fe(1)O_6$ and $Fe(2)O_6$ octahedra with light and dark shading respectively. The relative directions of the moments in the magnetically ordered phase below T_C are indicated as + or −.

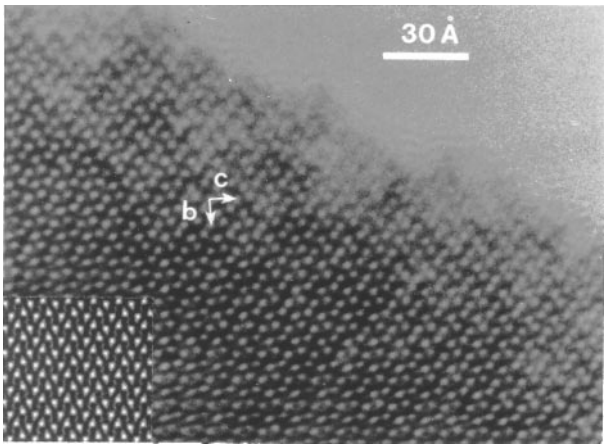

Fig. 4 A typical [100] HREM image of Fe_2OBO_3 with a calculated image inset (defocus value = 150 Å, thickness = 40 Å) showing dark/light contrast due mainly to the Fe/B atoms.

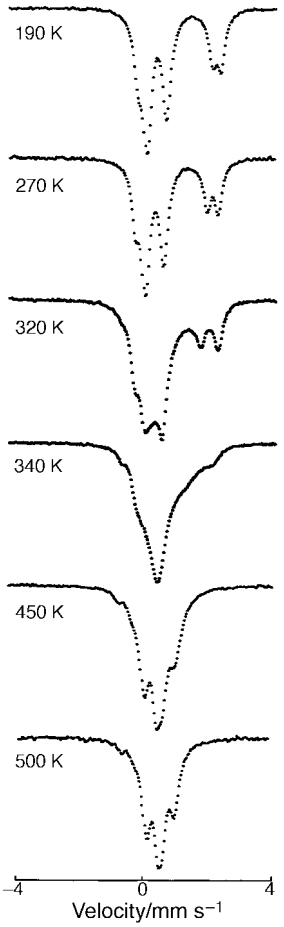

Fig. 5 Representative Mössbauer spectra of Fe_2OBO_3 between 190 and 500 K showing the change from slow to rapid electron hopping regimes.

on refined atomic parameters. The most precise (337 K) results are compared to the neutron parameters in Tables 1 and 3 showing that little structural change takes place at the monoclinic to orthorhombic transition.

Low temperature powder neutron diffraction

Constant wavelength neutron diffraction measurements were performed on the D2B high resolution diffractometer[16] at the ILL, Grenoble, France. Approximately 5 g of sample in an 8 mm diameter sealed vanadium can was used. Data were

Table 1 Refined atomic coordinates, temperature factors, magnetic moments and *R*-factors from Rietveld fits to neutron (3–190 K) and synchrotron X-ray (337 K) powder diffraction data. Magnetic moments at the Fe(1) sites are antiparallel to those at Fe(2) sites

	T/K						
	3	70	100	130	160	190	337
Fe(1): x	0.752(1)	0.754(2)	0.753(2)	0.748(3)	0.747(3)	0.752(1)	0.75
y	0.0667(3)	0.0669(3)	0.0661(3)	0.0681(4)	0.0675(5)	0.0667(3)	0.0690(3)
z	0.1169(3)	0.1169(3)	0.1165(4)	0.1174(5)	0.1174(6)	0.1168(3)	0.1176(4)
B_{iso}/Å^2	0.24(4)	0.27(5)	0.36(5)	0.48(8)	0.52(8)	0.49(5)	1.83(5)
Fe(2): x	0.248(1)	0.250(2)	0.248(2)	0.250(2)	0.247(2)	0.240(1)	0.25
y	0.1970(3)	0.1964(3)	0.1964(3)	0.1969(5)	0.1962(4)	0.1954(3)	0.1938(3)
z	0.3989(3)	0.3991(3)	0.3988(4)	0.3987(5)	0.3984(5)	0.3988(3)	0.3971(4)
B_{iso}/Å^2	0.22(4)	0.49(4)	0.57(5)	0.55(7)	0.40(7)	0.74(4)	1.83(5)
μ_x/μ_B	3.61(5)	3.47(5)	3.25(6)	2.28(8)			
μ_z/μ_B	−0.97 (19)	−0.88(24)	−0.74(30)	−0.23(67)			
μ/μ_B	3.74(4)	3.58(5)	3.33(5)	2.29(14)			
B: x	0.741(2)	0.742(2)	0.743(2)	0.748(3)	0.746(3)	0.748(2)	0.75
y	0.3763(6)	0.3760(7)	0.3747(7)	0.376(1)	0.377(1)	0.3769(6)	0.374(4)
z	0.1646(4)	0.1640(5)	0.1628(5)	0.1640(7)	0.1638(8)	0.1637(4)	0.167(2)
B_{iso}/Å^2	0.54(6)	0.63(7)	0.60(7)	0.2(1)	0.5(1)	0.63(6)	1.83(5)
O(1): x	0.238(2)	0.236(2)	0.239(2)	0.247(3)	0.249(3)	0.256(2)	0.25
y	0.1182(6)	0.1188(7)	0.1189(8)	0.1192(9)	0.117(1)	0.1181(7)	0.125(2)
z	0.9876(4)	0.9868(5)	0.9868(5)	0.9860(7)	0.9860(7)	0.9863(4)	0.973(2)
B_{iso}/Å^2	0.18(6)	0.40(7)	0.39(7)	0.3(1)	0.4(1)	0.65(6)	1.83(5)
O(2): x	0.234(2)	0.235(2)	0.239(3)	0.245(4)	0.256(4)	0.256(2)	0.25
y	0.0093(4)	0.0094(5)	0.0099(5)	0.0084(7)	0.0097(8)	0.0081(5)	0.001(2)
z	0.2677(5)	0.2657(6)	0.2652(6)	0.2639(8)	0.2628(8)	0.2654(5)	0.265(2)
B_{iso}/Å^2	0.17(7)	0.43(8)	0.32(8)	0.3(1)	0.2(1)	0.50(7)	1.83(5)
O(3): x	0.761(2)	0.759(3)	0.755(3)	0.764(4)	0.766(4)	0.751(3)	0.75
y	0.2498(4)	0.2508(5)	0.2516(5)	0.2516(7)	0.2530(8)	0.2521(5)	0.253(1)
z	0.2440(4)	0.2444(6)	0.2432(6)	0.2427(8)	0.2416(9)	0.2441(6)	0.244(1)
B_{iso}/Å^2	0.18(6)	0.53(8)	0.34(8)	0.3(1)	0.5(1)	0.70(8)	1.83(5)
O(4): x	0.740(2)	0.743(2)	0.742(2)	0.739(3)	0.738(4)	0.750(2)	0.75
y	0.3673(6)	0.3672(7)	0.3687(8)	0.367(1)	0.370(1)	0.3698(7)	0.388(2)
z	0.0186(4)	0.0188(5)	0.0188(5)	0.0173(8)	0.0169(8)	0.0180(5)	0.007(1)
B_{iso}/Å^2	0.58(6)	0.97(8)	1.05(9)	1.0(1)	1.2(1)	1.29(8)	1.83(5)
R_p (%)	6.3	7.4	8.0	10.6	11.1	6.6	16.6
R_{wp} (%)	8.5	9.5	10.1	13.5	13.9	8.1	26.9
RI_{nuc} (%)	10.4	9.4	11.2	12.4	14.0	12.5	
RI_{mag} (%)	11.4	12.4	15.0	23.4			
χ^2	7.28	2.05	1.73	1.03	1.10	3.41	0.90

Table 2 Refined lattice parameters for Fe_2OBO_3 from neutron (3–190 K) and synchrotron X-ray (291–337 K) powder diffraction

T/K	a/Å	b/Å	c/Å	β/°
3	3.16879(8)	9.3835(3)	9.2503(3)	90.220(1)
70	3.16929(9)	9.3838(2)	9.2497(3)	90.219(2)
100	3.1700(1)	9.3847(2)	9.2498(3)	90.220(2)
130	3.1715(2)	9.3846(4)	9.2483(5)	90.226(2)
160	3.1735(2)	9.3852(6)	9.2468(7)	90.249(2)
190	3.1750(1)	9.3878(3)	9.2469(4)	90.264(1)
291	3.181(3)	9.380(3)	9.257(8)	90.064(12)
312	3.181(2)	9.402(5)	9.258(5)	90.016(9)
315	3.184(1)	9.411(4)	9.266(4)	90
318	3.1825(6)	9.408(2)	9.263(2)	90
337	3.1779(1)	9.3945(1)	9.2495(1)	90

collected at 3, 70, 100, 130, 160 and 190 K over an angular range of 0–160° 2θ and with a neutron wavelength of 1.5946 Å. Magnetic peaks were observed below 160 K and the magnetic structure was found to be commensurate with the crystal cell, as reported previously.[17] Moments at the Fe(1) sites are antiparallel to those at the Fe(2) sites as shown in Fig. 3. Refinement results are shown in Tables 1–3.

High resolution electron microscopy (HREM)

Electron diffraction and HREM studies were performed on a 200 kV JEOL 2010 electron microscope. The EMS programs[18] were used to simulate lattice images using the multislice method for different crystal thicknesses. Reciprocal lattice reconstructions from electron diffraction patterns confirmed the pseudo-orthorhombic cell of Fe_2OBO_3 and no evidence for any supercell formation was observed. The [100] HREM image (Fig. 4) shows regular contrasts over large zones showing that the phase is well ordered with no intergrowths of other phases. Image simulations for defocus values of *ca.* 150 Å show the boron atoms as white regions between the black FeO_6 octahedra (*cf.* Fig. 3) and are in agreement with the observed image.

Mössbauer spectroscopy

^{57}Fe Mössbauer spectra were collected in transmission geometry using a conventional constant acceleration spectrometer and a ^{57}Co source diffused into a Rh matrix. A 5 mg Fe per cm^2 layer of powdered sample was placed in a He bath cryostat and an evacuated cryofurnace for low and high temperature experiments respectively. The low temperature spectra clearly reveal the presence of magnetic ordering. Representative spectra in the paramagnetic region are shown in Fig. 5.

From 190 to 270 K, the spectrum of Fe_2OBO_3 changes little and consists of two Fe^{2+} (isomer shift *ca.* 1.15 mm s^{-1}) and two Fe^{3+} (isomer shift *ca.* 0.35 mm s^{-1}) doublets, all of equal intensity. Between 270 and 380 K these signals broaden and

Table 3 Refined Fe–O and B–O distances (Å) for Fe_2OBO_3 from neutron powder diffraction (3–190 K) and synchrotron X-ray (337 K) powder diffraction

	T/K						
	3	70	100	130	160	190	337
Fe(1)–O(1)	2.074(6)	2.088(7)	2.080(8)	2.054(11)	2.044(11)	2.039(6)	2.004(7)
Fe(1)–O(1)	2.012(6)	2.009(7)	2.017(8)	2.055(11)	2.060(11)	2.064(6)	2.004(7)
Fe(1)–O(1)	1.986(6)	1.989(6)	1.981(7)	2.001(9)	1.979(10)	1.979(6)	1.987(18)
Fe(1)–O(2)	2.224(6)	2.215(8)	2.203(9)	2.171(12)	2.134(12)	2.169(7)	2.189(10)
Fe(1)–O(2)	2.134(6)	2.119(8)	2.126(9)	2.148(12)	2.166(12)	2.172(7)	2.189(10)
Fe(1)–O(3)	2.082(5)	2.091(6)	2.099(6)	2.077(8)	2.086(9)	2.101(5)	2.124(13)
Mean Fe(1)–O	2.085(2)	2.085(3)	2.084(3)	2.084(4)	2.078(4)	2.087(2)	2.083(4)
Fe(2)–O(1)	1.919(6)	1.916(7)	1.915(7)	1.905(10)	1.931(10)	1.930(7)	2.027(18)
Fe(2)–O(2)	2.139(5)	2.145(6)	2.143(6)	2.164(8)	2.153(9)	2.148(5)	2.184(12)
Fe(2)–O(3)	2.159(6)	2.171(9)	2.183(9)	2.169(12)	2.167(12)	2.173(7)	2.187(10)
Fe(2)–O(3)	2.227(6)	2.221(9)	2.222(9)	2.241(12)	2.263(12)	2.230(8)	2.187(10)
Fe(2)–O(4)	2.048(6)	2.044(8)	2.049(8)	2.051(12)	2.052(12)	2.008(7)	2.094(10)
Fe(2)–O(4)	2.002(6)	2.002(8)	2.010(8)	1.988(12)	2.002(12)	2.047(7)	2.094(10)
Mean Fe(2)–O	2.082(2)	2.083(3)	2.087(3)	2.086(4)	2.095(4)	2.089(3)	2.129(5)
B–O(2)	1.398(7)	1.413(8)	1.434(8)	1.411(12)	1.417(12)	1.396(7)	1.310(37)
B–O(3)	1.397(6)	1.391(8)	1.375(8)	1.375(12)	1.372(12)	1.387(7)	1.282(36)
B–O(4)	1.353(5)	1.346(6)	1.334(7)	1.359(10)	1.360(10)	1.349(6)	1.394(25)
Mean B–O	1.383(6)	1.383(7)	1.381(8)	1.382(11)	1.383(11)	1.377(7)	1.388(33)

coalesce due to the exchange of Fe^{2+} and Fe^{3+} environments through hopping of electrons between iron sites. Above 380 K, well defined Mössbauer lines are consistent with rapid electron hopping between two structurally distinct Fe sites.

Magnetisation

Magnetisation measurements were made using a Quantum Design SQUID magnetometer at fields of 0.05, 0.5 and 5 T. These reveal a magnetic ordering transition at $T_C = 155$ K, see Fig. 6. Although the neutron diffraction measurements showed an apparent antiferromagnetic ordering below T_C, the field dependence of the low temperature susceptibilities demonstrates that a ferromagnetically ordered component is also present. The maxima in the susceptibilities observed around 80 K at all three field strengths are characteristic of L-type ferrimagnetic order which is due to the 'up' and 'down' spins lying on structurally inequivalent Fe(1) and Fe(2) sites and so having slightly different saturation curves. This is also observed in $Fe^{III}_2(SO_4)_3$[19] and so is not a consequence of the mixed Fe valence in Fe_2OBO_3. The net magnetic moment at zero temperature is estimated to be 0.06 μ_B from the 0.05 T data, showing that the average spins at the two Fe sites are essentially of equal magnitude.

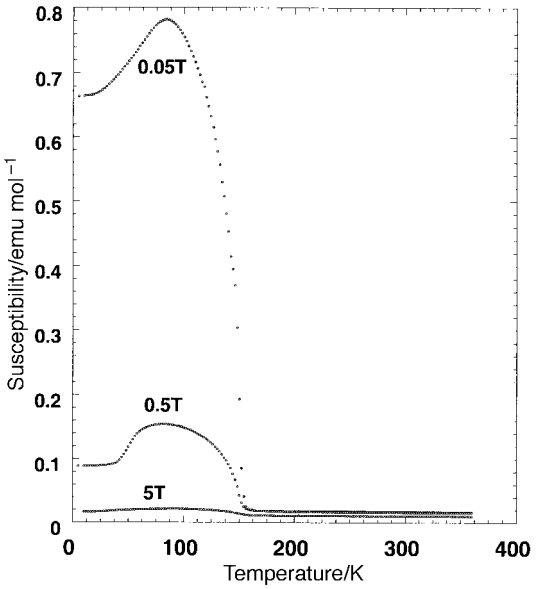

Fig. 6 Thermal variation of molar magnetic susceptibility for Fe_2OBO_3 in fields of 0.05, 0.5 and 5.0 T.

Resistivity

Four probe resistivity measurements (Fig. 7) were made on a sintered bar of Fe_2OBO_3 from 412 K to 240 K, below which the resistance was too large to be measured accurately. A broad semiconductor–semiconductor transition is observed around the monoclinic–orthorhombic structural transition at 317 K.

Conclusions

Fe_2OBO_3 can be prepared by solid state reaction without a flux or sample melting which tends to produce other iron oxoborates. A significant proportion of Fe_3O_4 is also produced, but this can be magnetically separated out. HREM shows that the Fe_2OBO_3 lattice is highly ordered with no intergrowths of other phases. A monoclinic–orthorhombic structural transition

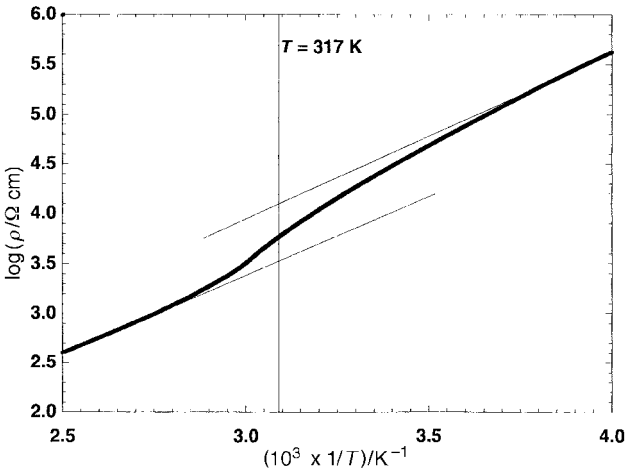

Fig. 7 Log(resistivity) plotted against inverse temperature with linear high and low temperature limits shown. The structural transition temperature of 317 K is marked.

occurs at 317 K, associated with an electronic transition between charge ordered and disordered states as evidenced by resistivity measurements and Mössbauer spectroscopy. This may be described as a less spectacular version of the Verwey transition in Fe_3O_4,[20] at which a sharp decrease in conductivity is accompanied by a complex structural distortion. Charge ordering in Fe_2OBO_3 accounts for the equal distribution of Fe^{2+} and Fe^{3+} over the two crystallographically distinct Fe sites resulting in equal mean Fe–O distances (Table 3). However, no long range Fe^{2+}/Fe^{3+} ordering is directly observed by X-ray, neutron or electron diffraction. A magnetic ordering transition at 155 K also occurs below which the magnetic structure is almost antiferromagnetic, but a small ferromagnetic component results from the inequivalence of the Fe sublattices giving an L-type ferrimagnetic behaviour overall.

We thank Drs. G. Bushnell-Wye (SRS), D. E. Cox (NSLS), and A. Hewat (ILL) for assistance with data collection. Support for A.M.T.B. from EPSRC and Daresbury Laboratory and for L.M.R.M. from the Basque Government is acknowledged.

References

1 E. F. Bertaut, *Acta Crystallogr.*, 1950, **3**, 473.
2 Y. Takeuchi, T. Watanabe and T. Ito, *Acta Crystallogr.*, 1950, **3**, 98.
3 F. Bertaut, L. Bochirol and P. Blum, *Compt. Rend.*, 1950, **230**, 764.
4 J. M. D. Coey, A. E. Berkowitz, L. Balcells, F. F. Putris and F. T. Parker, *Appl. Phys. Lett.*, 1998, **2**, 734.
5 J. P. Attfield, A. M. T. Bell, L. M. Rodriguez-Martinez, J. M. Greneche, R. J. Cernik, J. F. Clarke and D. A. Perkins, *Nature*, in press.
6 J. S. Swinnea and H. Steinfink, *Am. Mineral.*, 1983, **5**, 827.
7 K. Bluhm and H. K. Muller-Buschbaum, *Z. Anorg. Allg. Chem.*, 1990, **585**, 87.
8 K. Bluhm and S. Busche, *Z. Naturforsch. Teil B*, 1995, **50**, 1146.
9 M. J. Buerger and V. Venkatakrishnan, *Mater. Res. Bull.*, 1972, **7**, 1201.
10 K. Bluhm and A. Utzolino, *Z. Naturforsch. Teil B*, 1995, **50**, 1653.
11 K. Bluhm and A. Utzolino, *Z. Naturforsch. Teil B*, 1995, **50**, 1450.
12 J. H. Fang and R. E. Newnham, *Min. Mag. & J. Min. Soc.*, 1965, **35**, 196.
13 R. Norrestam, *Z. Kristallogr.*, 1989, **189**, 1.
14 R. Norrestam, M. Kritikos and A. Sjoerdin, *J. Solid State Chem.*, 1995, **114**, 311.
15 G. Bushnell-Wye and R. J. Cernik, *Rev. Sci. Instrum.*, 1992, **63**, 999.
16 A. W. Hewat, *Mater. Sci. Forum*, 1986, **9**, 69.
17 J. P. Attfield, J. F. Clarke and D. A. Perkins, *Physica B*, 1992, **180,** 581.
18 P. A. Stadelman, *Ultramicroscopy*, 1987, **21**, 131.
19 G. J. Long, G. Longworth, P. Battle, A. K. Cheetham, R. J. Thundathil and D. Beveridge, *Inorg. Chem.*, 1979, **18**, 624.
20 E. J. W. Verwey, *Nature*, 1939, **144**, 327.

Paper 8/04642E